American Mineralogist, Volume 91, pages 790–793, 2006

Site disorder revealed through Raman spectra from oriented single crystals: A case study on karooite ($MgTi_2O_5$)

HANNS-PETER LIERMANN,[1,2,*] ROBERT T. DOWNS,[3] AND HEXIONG YANG[2]

[1]High Pressure Collaboration Access Team (HPCAT) and Geophysical Laboratory, Advanced Photon Source, Argonne National Laboratory, Argonne, Illinois 60439, U.S.A.
[2]Center for the Study of Matter at Extreme Conditions (CeSMEC), Florida International University, Miami, Florida 33199, U.S.A.
[3]Department of Geosciences, University of Arizona, Tucson, Arizona 85721, U.S.A.

ABSTRACT

Raman spectroscopic data were collected from five oriented single crystals of karrooite ($MgTi_2O_5$) with different ordering states obtained by quenching crystals from 600, 700, 800, 1000, and 1400 °C. The Raman spectra were normalized and treated as vectors. The inner products among the Raman spectra are shown to correlate linearly with the ordered state of the crystals, suggesting that such an analysis of Raman spectra can, in principle, be used to rapidly estimate the ordering state of a mineral, and thus many other crystal properties related to the atomic order-disorder.

Keywords: Raman spectroscopy, cation ordering state, karooite, pseudobrookite

INTRODUCTION

Atomic order-disorder phenomena or intracrystalline atomic distributions play a key role in the energetics, crystal chemistry, and physical properties of numerous crystalline materials, including minerals (Hazen and Navrotsky 1996). They are a function of temperature, pressure, and chemical composition, and are related to the cooling history of host rocks (e.g., Ghose and Ganguly 1982; Hazen and Navrotsky 1996). In particular, the Fe^{2+}/Mg ordering states in orthopyroxenes have been used to constrain the thermal history of some meteorites (Ganguly 1982; Ganguly and Stimpfl 2000). The detailed knowledge of atomic order-disorder in minerals is generally retrieved with single-crystal X-ray diffraction. In the event that one of the Mars Rover missions will carry a miniature Raman spectrometer, a question has been raised whether one can collect Raman spectra on Mars, not only to identify minerals onsite, but also to estimate composition, compositional zoning, and order-disorder states of Martian minerals by comparing them against prerecorded Raman spectra from a database. Recent reports by Wang et al. (2001, 2004) and Huang et al. (2000) have shown that the bulk chemistry of silicates and oxide minerals can be estimated from Raman spectra. For example, the chemical composition of planetary quadrilateral Mg-Fe-Ca-Mn pyroxenes can be estimated to 3% through the analysis of their Raman spectra. The purpose of this paper is to provide a proof-of-concept demonstrating that Raman spectroscopy also can be used to quantify the ordering state in a mineral.

The cation occupancies at different crystallographic sites have been investigated by Boffa-Ballaran and Carpenter (2003) using infrared spectroscopy in solid solutions of omphacite, garnet, feldspar, amphiboles, and Fe^{2+}-Mg clinopyroxene. With the autocorrelation method of Salje et al. (2000), they evaluated effective line width variations of phonon bands in certain spectral intervals and related this to variations in site occupancies. For instance, the disorder of Mg and Fe^{2+} between the M1 and M2 sites in pyroxene corresponds to increased peak widths in the frequency range 210–800 cm^{-1}. The Al-Si disorder in feldspars is associated with broader peaks in the higher frequency regions related to tetrahedral bond stretching while the lower frequency modes associated with the alkali cation remain sharp. However, in garnet and amphibole, peak widths were found to increase in all regions of the spectrum, reflecting strain introduced by the increase in the degree of disordering.

Cynn et al. (1992, 1993) analyzed the Raman spectra of natural and synthetic spinels ($MgAl_2O_4$) taken in air in the temperature range from 25 to 961 °C. Their study indicates that the shape of the Raman peaks becomes asymmetric and broader as temperature increases. Furthermore, these features also can be observed at room-temperature conditions if the material is quenched rapidly from the highest temperature. Although their study did not directly relate the broadening and asymmetry of the Raman peaks to the order-disorder of Al/Mg between the octahedral and tetrahedral sites, the findings indicate that order-disorder has a systematic effect on Raman peak widths and positions and could be quantified if the width and positions of the vibration modes were analyzed appropriately.

To facilitate a proof-of-concept that the order-disorder state in minerals can be quantified from Raman spectra, we report the Raman spectra of karooite ($MgTi_2O_5$) as a function of Mg/Ti site occupancies. Karooite possesses a pseudobrookite structure and is an end-member of the solid solution between $MgTi_2O_5$ and $FeTi_2O_5$ (ferropseudobrookite). The intermediate member of this solid-solution series, armalcolite [~$(Fe,Mg)_2TiO_5$] (Anderson et al. 1970), received much attention during the Apollo missions because of its implications for the petrogenesis and cooling history of the lunar rocks (Haggerty 1973; Lind and Houseley 1972; Smyth 1974; Lindsley et al. 1974; Wechsler 1977). Karooite crystallizes in the space group *Bbmm*, and has two symmetrically nonequivalent edge-sharing octahedral sites, M1 and M2 (Fig.

* E-mail: pliermann@hpcat.aps.anl.gov

0003-004X/06/0506–790$05.00/DOI: 10.2138/am.2006.2027

1). When slowly cooled, the structure is well ordered with M1 predominately occupied by Mg and M2 by Ti. Neutron powder diffraction experiments by Wechsler and Von Dreele (1989) showed that quenching from high temperatures could induce disorder in karooite. Yang and Hazen (1998) conducted single crystal X-ray diffraction studies of Mg-Ti order-disorder in karooite as a function of quenching temperature. They showed that the disorder parameter, X = Ti (M_1) varies from 0.458(5) to 0.070(5) when the sample is quenched from temperatures ranging from 1400 to 600 °C.

Data collection and processing

Raman scattering was induced through the coherent light of a Ti-sapphire laser (Spectra Physics) tuned to a wavelength of 785 nm and filtered by a Kaiser Optics band-pass filter. Laser power for the excitation of Raman scattering was 50 mW. Raman spectra were collected in backscattering geometry on a Kaiser Optics holographic spectrometer equipped with a 1024–1024 thermoelectrically cooled CCD (Andor) calibrated with neon lines. Collection time for all spectra was 60 × 5 s (300 s). The experimental setup is illustrated in Figure 2.

The five single crystals of karooite used in this study were taken from Yang and Hazen (1998). The chemically identical crystals were quenched from temperatures of 1400, 1000, 800, 700, and 600 °C. All crystals were positioned on a glass slide with double-sided sticky tape with the **b**-axis oriented parallel to the laser beam and the **c**-axis vertical to assure that there were no spectral effects that could be ascribed to orientation. The recorded spectra are displayed in Figure 3 with inserts showing the oriented crystals. The positions of the Raman modes were determined by fitting three-parameter Gaussian functions to the intensity-wave number data as provided by the program "PeakFit." The refined positions of the individual modes, ν_i, of the crystals quenched from 600 and 1400 °C are listed in Table 1 and the behavior of the individual modes as a function of quenching temperature are illustrated in Figure 4. Linear fits to the peak positions are included as a guide for the eye.

Intensities above 1000 cm^{-1} were rather insignificant; so only 784 data points representing the spectra between 50–1000 Δcm^{-1} were used for the analysis of disorder. The spectra were therefore treated as 784 dimensional vectors, $\mathbf{S}^j$, with the i^{th} component of the vector representing the intensity recorded at the i^{th} pixel of the detector, and j representing the quenched temperature. Each spectrum was normalized such that the dot product with itself equals 100,

$$\mathbf{S}^j \cdot \mathbf{S}^j = \Sigma\, S^j_i \times S^j_i = 100.$$

The normalized spectra are displayed in Figure 3. Spectra can be compared with each other by finding the dot product of one vector with another. A perfect match produces a value of 100, whereas a complete mismatch with no common peak positions would produce a value of zero. In this way, spectral matches can be compared, quantified and ranked.

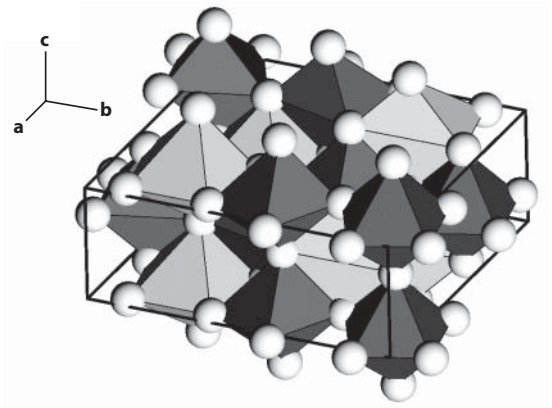

Figure 1. Structural image of karooite ($MgTi_2O_5$) that consists of two symmetrically distinct edge-sharing octahedral sites. When completely ordered, all Ti is located in the M2 site.

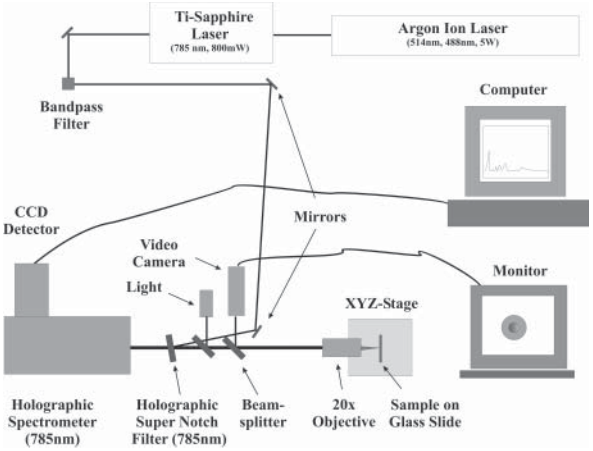

Figure 2. Schematic setup of the Raman system used to collect the spectra.

Results and discussion

For the orthorhombic structure of karooite, the theoretical analysis based on factor group analysis predicts a total of 48 normal modes:

$$\Gamma = 8A_g + 5B_{1g} + 3B_{1g} + 8B_{3g} + 3_{Au} + 8B_{1u} + 8B_{2u} + 5B_{3u}$$

Of these, 24 are Raman-active ($8A_g + 5B_{1g} + 3B_{1g} + 8B_{3g}$) and 21 are infrared-active ($8B_{1u} + 8B_{2u} + 5B_{3u}$). The spectra collected from the single crystals quenched at 600 and 1400 °C show a total of 21 and 20 discernible modes, respectively (Table 1; Figs. 3 and 4). Figure 4 indicates that some modes (ν_7, ν_{12}, ν_{15}, and ν_{20}) are not visible in the spectrum of the crystal quenched from 600 °C because they were too weak or they overlap with stronger peaks. Furthermore, the spectrum collected from the crystal quenched from 1400 °C indicates that modes ν_{11}, ν_{12}, ν_{13}, and ν_{14} as well as modes ν_{21} and ν_{22} merge into one another between 600 and 1400

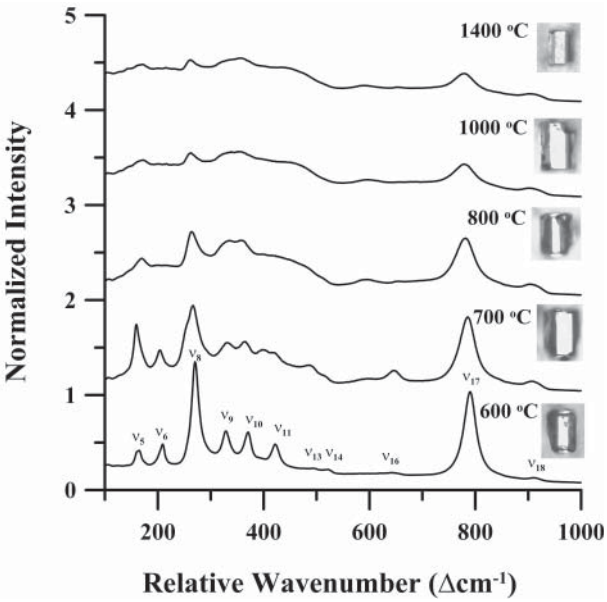

Figure 3. Raman spectra of karooite ($MgTi_2O_5$) normalized and stacked with the most ordered state at the bottom of the plot.

TABLE 1. List of refined positions of ν_i vibration modes of oriented crystals of karooite ($MgTi_2O_5$) quenched from 600 and 1400 °C, as illustrated in Figure 3

Modes	600 (°C)	1400 (°C)
ν_1	87.6(4)	–
ν_2	105(1)	106.7(9)
ν_3	124(3)	127(1)
ν_4	140(2)	142.3(7)
ν_5	165.3(3)	168(1)
ν_6	206.8(3)	198(1)
ν_7	–	260.7(5)
ν_8	270.34(3)	274(2)
ν_9	329.1(1)	323.8(8)
ν_{10}	369.9(1)	356(1)
ν_{11}	421.9(1)	448(2)
ν_{12}	–	–
ν_{13}	499(13)	–
ν_{14}	522(1)	–
ν_{15}	–	593(3)
ν_{16}	632(1)	653(3)
ν_{17}	789.92(1)	779.2(1)
ν_{18}	913.0(2)	908.7(4)
ν_{19}	1041.8(1)	1040.8(2)
ν_{20}	–	1080(1)
ν_{21}	1112(4)	1156(2)
ν_{22}	1165.1(6)	–
ν_{23}	1253(8)	1223(1)
ν_{24}	1366(1)	1365.4(7)
ν_{25}	1446(1)	1506(3)

Notes: The values in parentheses represent the estimated standard deviation (e.s.d.) in terms of the least units cited for the value to the immediate left; thus 87.6(4) indicates an e.s.d. of 0.4.

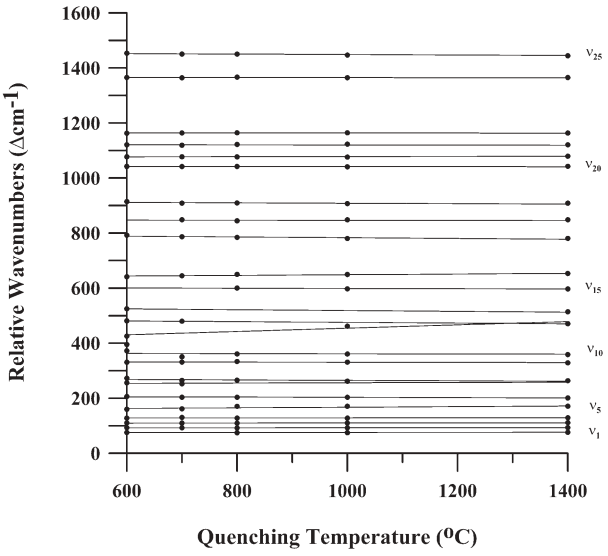

FIGURE 4. Summary of variation in the refined positions of the Raman peaks in karooite ($MgTi_2O_5$) as a function of quenching temperature.

°C (Fig. 4). This observation is consistent with that made by Cynn et al. (1992) that disorder is associated with peak broadening. We interpret the broadening as due to mode splitting driven by the various short-ranged distributions of Mg and Ti octahedral occupancies that result from the disorder.

Table 2 contains a list of the dot products between the vectorized spectra. The dot products between $\mathbf{S}^{600}$ and the other spectral vectors as a function of the disorder parameter X_{Ti}(M1) (Yang and Hazen 1998) is plotted in Figure 5A. For comparison, the disorder parameter X_{Ti}(M1) as a function of quenching temperature, is shown in Figure 5B. As $\mathbf{S}^{600}$ is located at one end of the

TABLE 2. Dot products of vectorized Raman spectra from single crystals of karooite ($MgTi_2O_5$) quenched between 600 and 1400 °C

Dot Products	SP (600)	SP (700)	SP (800)	SP (1000)	SP (1400)	X_{Ti}(M1)
SP (600)	100.00	96.97	94.61	90.86	89.80	0.070
SP (700)		100.00	98.07	94.99	94.00	0.203
SP (800)			100.00	98.24	97.34	0.306
SP (1000)				100.00	99.58	0.404
SP (1400)					100.00	0.485

Notes: Values of 100 indicate a perfect match whereas those with a value of zero show no match at all. For comparison the disorder parameter X_{Ti}(M1) as determined from Yang and Hazen (1998) is plotted in the last column.

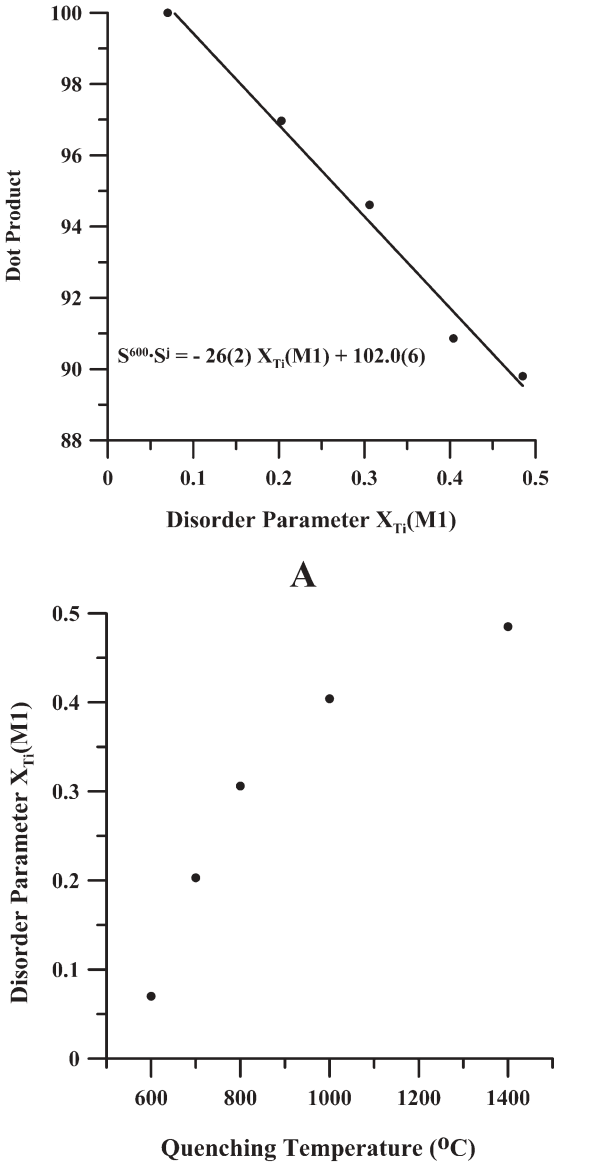

FIGURE 5. Disorder parameter X_{Ti}(M1) as a function of dot product between the spectrum vectors (**A**) and as a function of quenching temperature (**B**) (Yang and Hazen 1998). Equation and solid line in **A** indicates linear least-square regression through the dot products as a function of disorder parameter.

temperature range, the dot products, $\mathbf{S}^{600} \cdot \mathbf{S}^{j}$ covers the entire range of observed values. $\mathbf{S}^{600} \cdot \mathbf{S}^{j}$ displays a value of 100 when $j = 600$, and decreases monotonically to a value of 89.9 when $j = 1400$. Linear least-squares regression through the values of the dot products as a function of the disorder parameter results in $\mathbf{S}^{600} \cdot \mathbf{S} = -26(2)\, X_{\mathrm{Ti}}(\mathrm{M1}) + 102.0(2)$, with $R = 0.99$, as indicated in Figure 5A. The regular and linear trend indicates that Raman spectra are capable of providing a quantitative measure of the disorder in a mineral.

To estimate the reliability of this calibration, the dot product of the normalized spectrum quenched from 700 °C was calculated and is used as an example. Substituting the value for $\mathbf{S}^{600} \cdot \mathbf{S}^{700}$ returns a disorder parameter of $X_{\mathrm{Ti}}(\mathrm{M1}) = 0.205$, which is in very good agreement with the disorder parameter of 0.203(3), determined by Yang and Hazen (1998) for samples quenched at 700 °C, with a difference of $\Delta X(700) = 0.008$.

In general, however, a complete calibration of spectra with different disorder parameters is not likely to be available in a database for all minerals of interest. In such a case, it is envisioned that the unknown spectrum can be dotted with the others that are available and the comparison of the respective dot products can provide an estimate of its disorder. For instance, the dot product of $\mathbf{S}^{700}$ relative to $\mathbf{S}^{600}$ and $\mathbf{S}^{800}$ results in $X_{\mathrm{Ti}}(\mathrm{M1}) = 0.215$, with a difference of $\Delta X(700) = 0.011$. This indicates that even if a well-calibrated analytical expression is not available, the order-disorder state still can be estimated with reasonable accuracy.

The above vector analysis of the Raman spectra of karooite crystals with different ordering states demonstrates that Raman spectroscopy may be used to estimate ordering states in minerals, and thus cooling rates of their host rocks. Of particular interest is that the in situ application of this analytical technique to extraterrestrial rocks through Raman probes that can be installed on unmanned spacecraft seems to be within reach. Nonetheless, the successful implementation of this technique for measurements of ordering states would require the detailed knowledge of crystallographic orientations of minerals in question and the expansion of the database to include a calibration of the more commonly found rock-forming minerals such as orthopyroxene and spinel.

REFERENCES CITED

Anderson, A.T., Crewe, A.V., Goldsmit, J.R., Moore, P.B., Newton, J.C., Olsen, E.J., Smith, J.V., and Wyllie, P.J. (1970) Petrological history of the Moon suggested by petrography, mineralogy, and crystallography. Science, 167(3918), 587–588.

Boffa-Ballaran, T. and Carpenter, M.A. (2003) Line broadening and enthalpy: Some empirical calibration of solid-solution behavior from IR spectra. Phase Transitions, 76, 137–154.

Cynn, H., Sharma, S.K., Cooney, T.F., and Nicol, M. (1992) High-temperature Raman investigation of order-disorder behavior in the $MgAl_2O_4$ spinel. Physical Review B, 45, 500–502.

Cynn, H., Anderson, O.R., and Nicol, M. (1993) Effects of cation disordering in a natural $MgAl_2O_4$ Spinel observed by rectangular parallelepiped ultrasonic resonance and Raman measurements. Pure and Applied Geophysics, 141, 415–444.

Ganguly, J. (1982) Mg–Fe order-disorder in ferromagnesian silicates: II. Thermodynamics, kinetics and geological applications. In S.K. Saxena, Ed., Advances in Physical Geochemistry, vol. 2, p. 1–99. Springer-Verlag, New York.

Ganguly, J. and Stimpfl, M. (2000) Cation ordering in orthopyroxenes from two stony-iron meteorites: Implications for cooling rates and metal-silicate mixing. Geochimica et Cosmochimica Acta, 64, 1292–1297.

Ghose, S. and Ganguly, J. (1982) Mg-Fe order-disorder in ferromagnesian silicates. In S.K. Saxena, Ed., Advances in Physical Geochemistry, vol. 2, p. 1–99. Springer-Verlag, New York.

Haggerty, S.E. (1973) Ortho and para-armalcolite samples in APOLLO 17. Nature, 242, 123–125.

Hazen, R.M. and Navrotsky, A. (1996) Effects of pressure on order-disorder reactions. American Mineralogist, 81, 1021–1035.

Huang, E., Chen, C.H., Huang, T., Lin, E.H., and Xu, Ji-An (2000) Raman spectroscopic characteristics of Mg-Fe-Ca pyroxenes. American Mineralogist, 85, 473–479.

Lind, M.D. and Houseley, R.M. (1972) Crystallization studies of lunar igneous rocks: Crystal structure of synthetic armalcolite. Science, 175, 521–523.

Lindsley, D.H., Kesson, S.E., Hartzman, M.J., and Cushman, M.K. (1974) The stability of armalcolite: Experimental studies in the system MgO-Fe-Ti-O. Proceedings of the 5th Lunar Science Conference, Geochemica et Cosmochemica Acta Supplement, 61, 521–534.

Salje, E.K.H., Carpenter, M.A., Malcherek, T.G.W., and Boffa Ballaran, T. (2000) Autocorrelation analysis of infrared spectra from minerals. European Journal of Mineralogy, 12, 503–519.

Smyth, J.R. (1974) The crystal chemistry of armalcolite from Apollo 17. Earth and Planetary Science Letters, 24, 262–270.

Wang, A., Jolliff, B.L., Haskin, L.A., Kuebler, K.E., and Viskupic, M. (2001) Characterization and comparison of structural and compositional features of planetary quadrilateral pyroxenes by Raman spectroscopy. American Mineralogist, 86, 790–806.

Wang, A., Kuebler, K.E., Jolliff, B.L., and Haskin, L.A. (2004) Raman spectroscopy of Fe-Ti-Cr-oxides, case study: Martian meteorites EETA79001. American Mineralogist, 89, 665–680.

Wechsler, B.A. (1977) Cation distribution and high-temperature crystal chemistry of armalcolite. American Mineralogist, 62, 913–920.

Wechsler, B.A. and Von Dreele, R.B. (1989) Structure refinements of Mg_2TiO_4, $MgTiO_3$ and $MgTi_2O_5$ by time-of-flight neutron powder diffraction. Acta Crystallographica, B45, 542–549.

Yang, H. and Hazen, R.M. (1998) Crystal chemistry of cation order-disorder in pseudobrookite-type $MgTi_2O_5$. Journal of Solid State Chemistry, 138, 238–244.

MANUSCRIPT RECEIVED JULY 1, 2005
MANUSCRIPT ACCEPTED NOVEMBER 9, 2005
MANUSCRIPT HANDLED BY BRIGITTE WOPENKA